Int. J. Electrochem. Sci., 10 **(2015)** 6187 - 6198

International Journal of
ELECTROCHEMICAL
SCIENCE
www.electrochemsci.org

Comparative Study of the Behavior of API 5L-X65 Grade Steel and ASTM A53-B Grade Steel against Corrosion in Seawater

Rosa Vera[*], *Fabrizio Vinciguerra, Margarita Bagnara*

Institute of Chemistry, Faculty of Sciences, Pontificia Universidad Católica de Valparaíso,
Av. Universidad 330, Placilla (Curauma), Valparaíso, Chile.
[*]E-mail: rvera@ucv.cl

Received: 18 February 2015 / *Accepted:* 2 June 2015 / *Published:* 24 June 2015

Low freshwater availability in northern Chile means that many mining companies use seawater for several different processes. The present study analyzes the corrosion behavior of API 5L X65 steel and ASTM 53-B steel in seawater taken from the coast of northern Chile. Electrochemistry (polarization curves) and mass loss (flow simulation) techniques are used. The results obtained from the (static) electrochemical testing give the corrosion potential, corrosion current, corrosion rate, passivity current and pitting potential. All measurements show improved corrosion behavior in seawater for the API 5L X65 steel. The total corrosion rate, which includes the corrosion and erosion processes for the materials in the flow simulation system, was 0.41 μm $year^{-1}$ at day 10 for the API 5L X65 steel and 0.59 μm $year^{-1}$ at day 10 for the ASTM A53-B steel. Scanning microscopy observations show the presence of pitting, more so for the ASTM A53-B steel.

Keywords: corrosion, API 5L X65 carbon steel, ASTM A53-B carbon steel, seawater, mining

1. INTRODUCTION

The limited availability of freshwater in northern Chile has affected the mining industry, restricting its possibilities for expansion and the development of new projects due to a lack of this essential resource. As a result, the use of seawater in mineral processes, which once seemed novel, is today practically obligatory for the mining industry. It has progressively increased in recent years with alternatives that include desalination as well as direct use without prior treatment.

Seawater is an extremely abundant and corrosive electrolyte of natural origin. It has a high concentration of salts, mainly in the form of chlorides, and covers approximately 70% of the surface of the earth. The aggressive nature of the medium generates high corrosion rates on metals and alloys commonly used in structures and transport systems. In addition, considering the relative motion of a

corrosive fluid and the metallic material submerged in it, the surface of the material is also exposed to the effects of mechanical wear, a process known as erosion corrosion and the loss of the material is greater in this case than damage produced by erosion and corrosion individually [1-10].

Due to the aggressive nature of the aqueous environment in different parts of an industrial plant, a material's corrosion resistance has become of vital importance. Given that more durable materials are generally more expensive corrosion resistance is a crucial component of the debate on the impact of selecting certain materials with regard to capital and operational costs in industry.

This has led to increased demand for high-strength steels for the construction of pipelines; examples of such steels are API 5L X65 grade and ASTM A53-B grade. It has been shown that the manufacture of these types of steels requires a strict procedure, controlled hot rolling followed by accelerating cooling of the deformed plate [11-12]. The addition of micro-alloying elements gives an improved response during subsequent processing. For example, the reduction of carbon content (<0.05% in weight) improves solubility and reduces hardness of the area affected by the heat. It has been found that low sulfur content decreases susceptibility to hydrogen-induced cracking and that low phosphorus content reduces hardening in segregated regions [13-14].

API 5L X65 steel is the most widely accepted material for these types of pipes, which require a special limits of formability and strength. These pipes are manufactured with microalloyed steel using elements such as Niobium, Titanium, Vanadium and low Carbon content (0.1% in weight), giving the steel resistance, strength and weldability. A controlled thermo-mechanical rolling process is used to control grain refinement and strengthen the material [15-19].

The alloying of ASTM A53-B grade carbon steel is aimed at mechanical and high pressure applications. It is also acceptable for common uses on vapor, water, gas and air pipelines. Such a pipe system is adequate for welding and other forming operations such as rolling, folding and forming flanges. Together with API 5L X65 steel, they are produced with micro-alloying steel containing elements such as Manganese, Chromium, Vanadium and with low Carbon content [20].

However, the current focus of the manufacture of these materials and studies from an engineering perspective are generally aimed at achieving improved strength. Given that copper producers in Chile use pipes made from these materials, the objective of the present study is to evaluate and compare the corrosion resistance of API 5L X65 and ASTM A53-B grade carbon steel alloys in seawater from northern Chile, using electrochemistry and mass loss techniques.

2. MATERIALS AND METHODS

2.1. Materials and electrolyte

Table 1 presents the chemical composition of the steels used in this study, found using optical emission spectroscopy.

Table 1. Chemical composition of tested steels (%).

	C	Si	Mn	P	S	Cr	Ni	Mo	Al
API 5L X65	0.094	0.195	1.420	0.011	0.004	0.19	<0.0025	0.003	0.34
ASTM A53-B	0.077	0.026	0.198	0.005	0.009	0.026	0.007	0.003	0.005

	Cu	Co	Ti	Nb	V	W	Sn	B
API 5L X65	0.009	0.004	0.005	0.034	0.003	<0.0070	0.009	0.0014
ASTM A53-B	0.015	0.004	<0.0005	<0.004	0.002	0.013	0.020	0.0013

*Fe balance

The percentage of carbon places the steel in the category of low carbon, high strength, high ductility and high plastic deformation capacity.

The electrolyte used in the tests is seawater from northern Chile in order to simulate the real conditions to which steel pipes are exposed in the mining industry. The characteristics of the electrolyte are as follows: chlorinity 19.64 g Kg^{-1}, salinity 35.45 g Kg^{-1}, conductivity 45.40 mS cm^{-1} and pH 7.73. The mean chlorinity and salinity values are slightly higher than worldwide averages, which are 19.37 g Kg^{-1} and 35.16 g Kg^{-1}, respectively [21].

2.2 Micro-structure and hardness

The metallographs for each steel were obtained using Nital at 10% as the attack reagent and the grain size was determined in accordance with ASTM E 112-96 [22]. The hardness of the materials was measured with a Rockwell hardmeter with a load of 60 kg of pressure.

2.3 Electrochemical testing

The corrosion potential of the materials was measured using a G-SEC V2.0 potentiostat-galvanostat and a saturated calomel reference electrode. In order to obtain the polarization curves, a platinum wire counter-electrode was added to the system. The surface area of the test probes was 1 cm^2. The polarization curves were obtained in an aerated solution at 25 °C and at a scan rate of 0.2 mV s^{-1}. The attack morphology was observed with a Carl Zeiss Evo MA 10 scanning electron microscope (SEM).

2.4 Corrosion testing in flow system

The study was carried out at 20 °C in a closed flow rack system with a capacity of 25 liters and a flow rate of 20.0 L/min, in accordance with ASTM D 2688-94 [23]. The area of the probes was 33 cm^2 and 15 cm^2 for the API 5L X65 and ASTM A53-B steels, respectively. The corrosion was evaluated through mass loss measurements in accordance with ASTM G1-03 [24] and the attack morphology was observed through photographs and SEM.

3. RESULTS AND DISCUSSION

3.1 Material characteristics

From Table 1 it can be seen that the chemical composition of the API 5L X65 steel used in pipes in Chile has a larger amount (% in weight) of elements such as manganese (Mn), titanium (Ti), niobium (Nb) and vanadium (V), in comparison to the ASTM A53-B steel. These components are fundamental to both materials for forming alloys that comply with the role of pipes and transport lines, as these alloying elements give the material a good combination of strength, hardness and toughness [16, 19]. In addition, Mn, Ti, Nb and V together with aluminum and chromium improve the corrosion resistance of these materials, favoring the steels' passivity.

Fig. 1 shows the microstructure of the API 5L X65 grade steel and the ASTM A53-B grade steel used in this study. Both are formed principally from ferrite grains. The grain size was measured at ASTM 10 for the API steel, classifying it as quite fine, and at ASTM 8 for the ASTM steel, classifying it as a fine grain size. The presence of low quantities of niobium, titanium and vanadium in the steel composition generates these fine structures [19, 22].

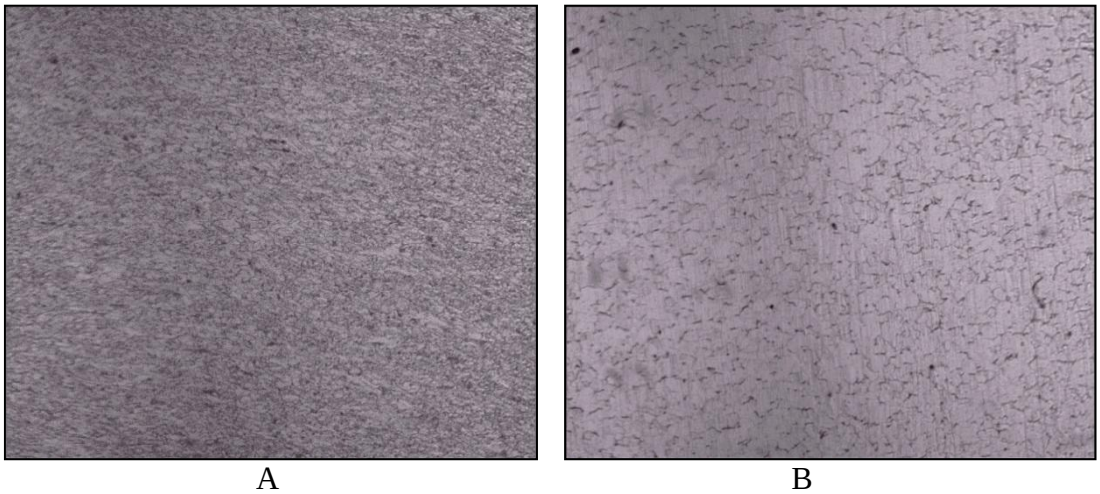

Figure 1. Microstructure of API 5L X65 grade steel (A) and ASTM A53-B grade steel (B), 200x.

The hardness test gave results of average values of 54.0 HR_A and 42.8 HR_A for the API 5L X65 and ASTM A53-B, respectively. This confirms the classification of API 5L X65 steel as a high strength pipe material and the ASTM A53 steel as medium strength. This variable is of vital importance when considering transport line wear due to corrosion/erosion.

3.2 Electrochemical testing

3.2.1 Corrosion Potential

Fig. 2 shows the variation in corrosion potential for the alloys as a function of time in aerated conditions. For both steels, the trend over time is to decrease corrosion potential, showing the materials' dissolution capacity in seawater, reaching values of -706.5 mV_{ecs} for API 5L X65 and -715.8 mV_{ecs} for the ASTM A53-B. However, from 20 minutes onwards, at a potential of -715.8 mV_{ecs} the ASTM A53-B steel increases its potential by approximately 20 mV_{ecs}, thus corroborating the formation of a passive corrosion product. Similar behavior is seen for the API 5L X65 steel at 30 minutes.

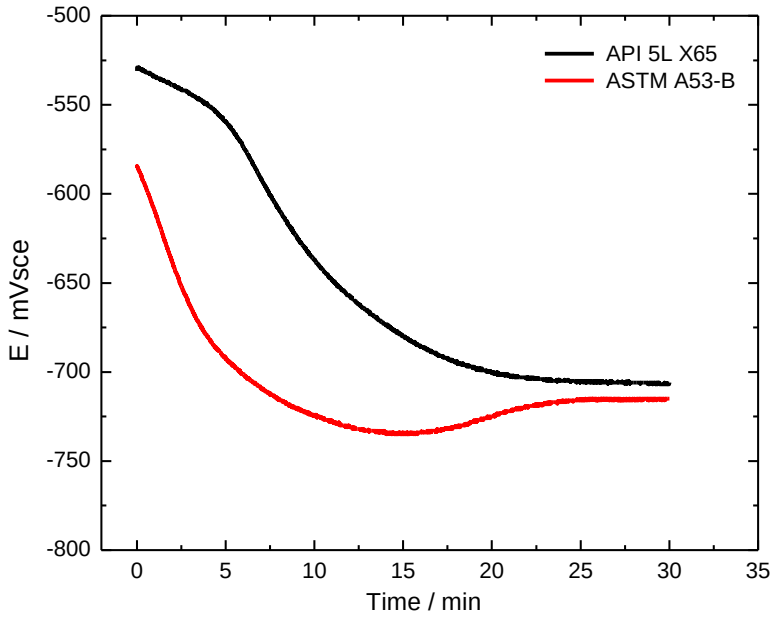

Figure 2. Corrosion potential as a function of time. API 5L X65 and ASTM A53-B in seawater.

Corrosion potential depends on the characteristics of the material in question and the composition of the electrolyte. The electrochemical and chemical reactions that occur under these conditions are shown in equations 1 to 6.

anodic reaction: $Fe_{(s)} \rightarrow Fe^{+2}_{(ac)} + 2e^-$ (1)

cathodic reaction: $O_{2(g)} + 2H_2O_{(l)} + 4e^- \rightarrow 4OH^-_{(ac)}$ (2)

total reaction: $2Fe_{(s)} + O_{2(g)} + 2H_2O_{(l)} \rightarrow 2Fe^{+2}_{(ac)} + 4OH^-_{(ac)}$ (3)

$$Fe^{+2}_{(ac)} + 2OH^{-}_{(ac)} \rightarrow Fe(OH)_{2(s)} \quad (4)$$

$$4Fe(OH)_{2(s)} + O_{2(g)} + 2H_2O_{(l)} \rightarrow 4Fe(OH)_{3(s)} \quad (5)$$

$$2Fe(OH)_{3(s)} \rightarrow Fe_2O_3 \cdot H_2O_{(s)} + 2H_2O_{(l)} \quad (6)$$

3.2.2 Polarization Curves

Fig. 3 shows the polarization curves (Evans diagrams) used to compute the electrochemical variables, corrosion potential (Ec), corrosion current (Ic), corrosion rate (Vc) and pitting potential (Ep) (Table 2). The anodic curves show, initially, an active dissolution zone (ec. 1), subsequently, both curves exhibit a passive zone in a potential range from -600 mVsce to -360 mVsce (Ec. 4, 5 and 6) and finally, a pitting zone appears in a potential over -300 mVsce and currents higher than 1.0 x 10^{-4} A cm^{-2}, corresponding to the dissolution of Fe_2O_3, generating iron ions in the solution again [25-26]. The cathodic curve corresponds to the oxygen reduction (ec. 2).

The results show that the values obtained for Ic and Vc show better behavior for corrosion in seawater for the API 5L X65 steel. Both steels have a low degree of alloying, however, the presence of a higher Cr, Nb, Mn and Al content and a finer grained microstructure in the API 5L X65 give it better behavior under corrosion. This is confirmed by the calculations for passivity current (Ip) for both steels at a potential of -500.0 mVsce, where the ASTM A53-B steel has an Ip value that is twice that obtained for the API 5L X65 steel.

The data obtained for pitting potential is similar for the two steels, with a difference in value of only 36 mV. Fig. 4 shows the surface appearance of the samples after completion of the anodic curves (currents in the region of 10^{-2} A cm^{-2}), showing the presence of pitting across the entire surface of both steel types.

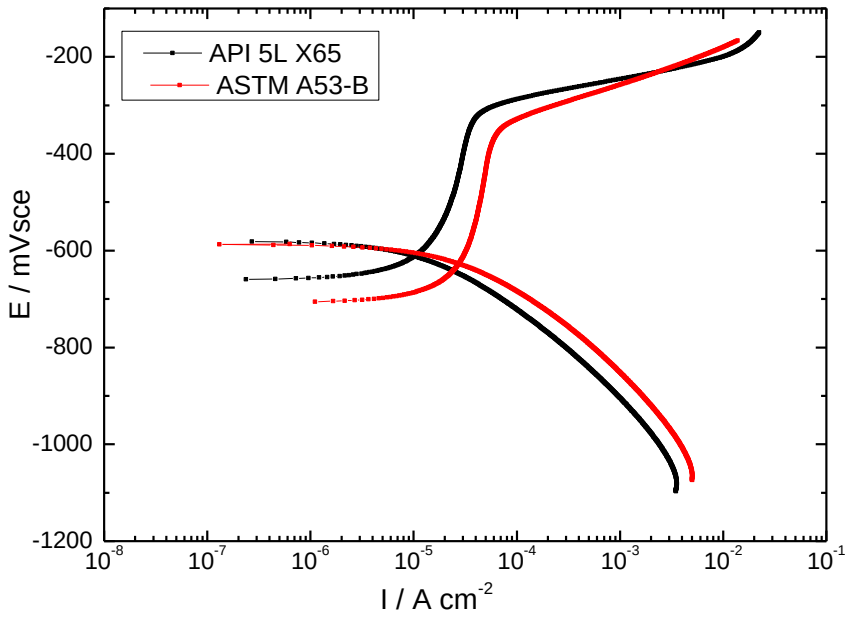

Figure 3. Evans Diagram for the API 5L X65 and ASTM A53-B steel in seawater.

Table 2. Electrochemical variables for the API 5L X65 and ASTM A53-B steel in seawater.

Samples	Ec (mV)	Ic (A cm^{-2})	Vc (mm $year^{-1}$)	Ep (mV)	Ip at -500 mV (A cm^{-2})
API 5L X65	-610.9	1.03×10^{-5}	0.120	-318.3	2.29×10^{-5}
ASTM A53-B	-628.6	2.84×10^{-5}	0.330	-354.0	4.59×10^{-5}

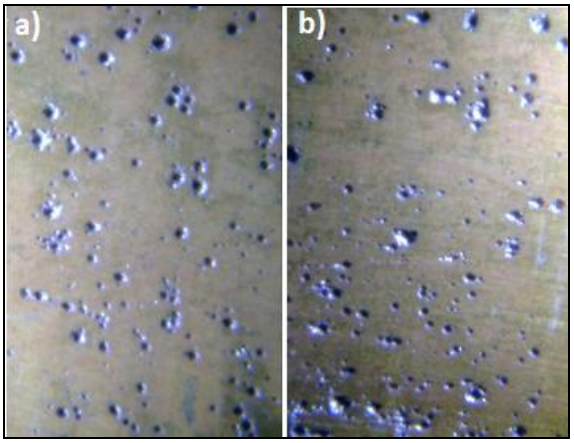

Figure 4. Surface appearance of the sample after the anodic curve. a)API 5L X65 b) ASTM A53-B.

3.3 Corrosion testing in a flow system

The results obtained from the corrosion testing in a flow simulator are in agreement with those obtained in the electrochemical testing, showing better behavior for the API 5L X65 steel.

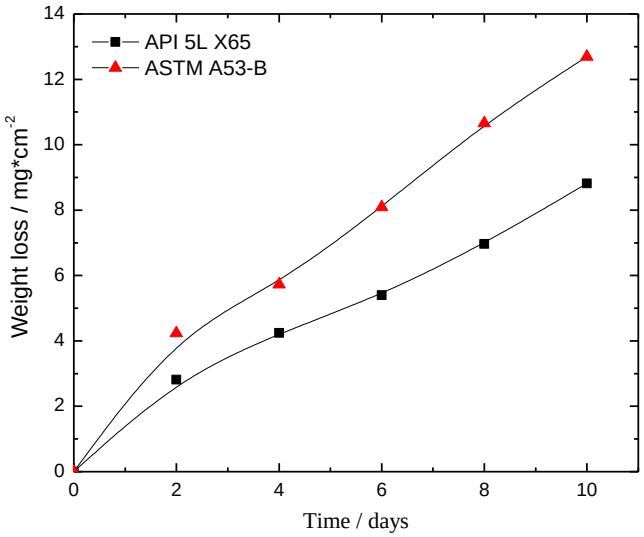

Figure 5. Mass loss variation over time for the API5L X65 and ASTM 53-B steels.

Fig. 5 shows the variation in mass loss as a function of time for the two steels. An increasing trend can be seen for this variable, with a higher slope for the A53-B steel. Table 3 shows the long term prediction models given by the function $WL = A*t^n$. This model can also be represented by a bilogarithmic model, $\log_{10}\mathbf{C} = \mathbf{n}\cdot \log_{10}\mathbf{t} + \log_{10}\mathbf{A} + \varepsilon$, where for the conditions used in this study: *WL* is the mass loss per unit of years (mg cm^{-2}), *t* is the testing time in days, *A* is the mass loss on the first day and *n* is an index of the physical/chemical behavior of the corrosion layer and its interactions with the aggressive medium. The value of n depends in general on the type of metal or alloy, on the medium in which the material is exposed and on the exposure conditions. The higher value of n for the ASTM A53-B steel is associated with the lower protective nature of the corrosion products formed on this material.

Table 3. Estimated prediction models for the behavior of the steels.

Sample	Model as a function of time	R^2
API 5L X65	WL = 0.8240 * t + 0.5863	97.75
ASTM A53-B	WL = 1.2159 * t + 0.8211	97.94

Fig. 6 shows the variation in total corrosion rate during the 10 days of testing. The position of the test probe in the flow simulator was parallel to the electrolyte flow; therefore the total rate considers the rate due solely to corrosion, solely to erosion and to a synergy between corrosion and erosion. It is important to note that the loss of the material due to corrosion depends on the angle of exposure with regard to the direction of electrolyte flow, due to the change in direction of the movement and due to the distribution of solid particles on the material surface [4, 27-29]. The erosion process also accelerates mass transport, eliminating corrosion products and increasing the roughness of the metal surface, thus increasing the corrosion rate.

The data obtained are in agreement with the results described above, i.e. the total corrosion rate is lower for the API 5L X65 steel. However, for both steels the values obtained in the flow test are higher than those from the polarization curves (point 3.2.2), where the test is conducted under static conditions. It can also be seen that as of the sixth day of testing, both steels reach a constant corrosion rate, due to the formation of corrosion products on their surface (preferentially forming Fe_2O_3 rust). The chromium content in the composition of the API steel favors the formation of a more protective and more adherent corrosion product.

Fig. 7 shows the test probes of both steels after the corrosion testing at different times. The formation of a more voluminous corrosion product from day six onwards is responsible for the loss of adherence of the corrosion product on the metal base, showing a higher level of loss for the ASTM A53-B steel. Cross-section observations using SEM at day 10 of the flow testing show a more general corrosion attack morphology for the API 5L X65 steel (Fig. 8A), with a layer of homogenous corrosion product measuring 25 to 35 μm in thickness, with small fissures and loss of adherence of the outer rust layer.

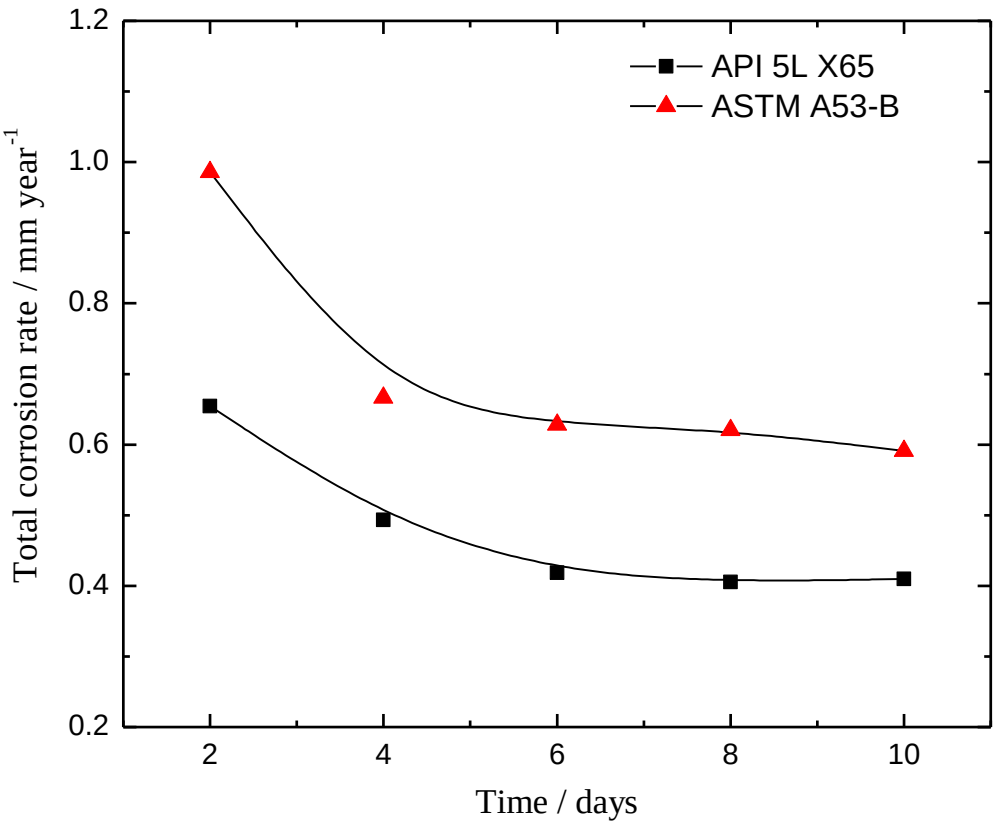

Figure 6. Total corrosion rate as a function of time.

For the ASTM A53-B steel, the corrosion attack morphology shows a higher degree of pitting, fissures and lack of adherence of the corrosion product, while also showing the same loss of adherence of the outer layer of corrosion product, mainly due to the corrosion/erosion process (Fig. 8B). The existence of bare areas on the material due to erosion (anodic zones) and areas with corrosion product (cathodic zones) leads to the formation of a galvanic couple that increases the corrosion rate in both materials, though more so for the ASTM A53-B.

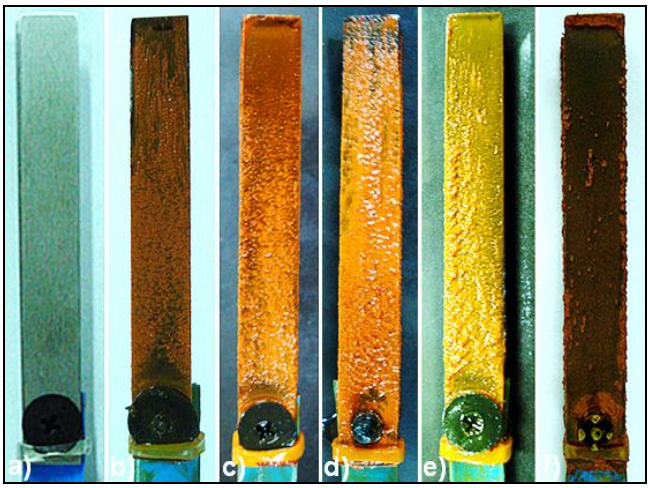

A

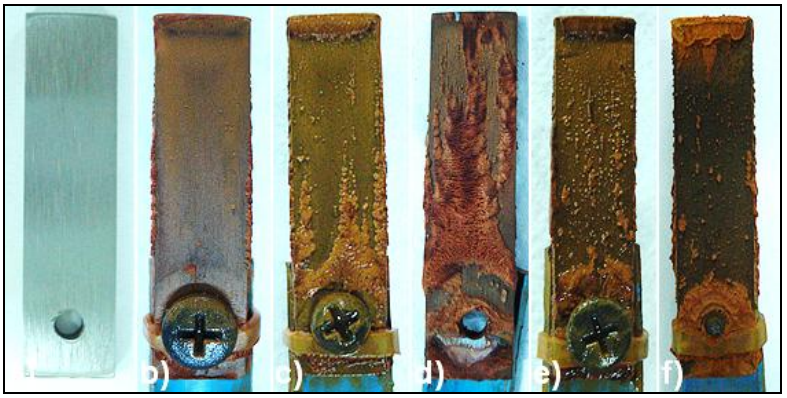

B

Figure 7. Samples exposed in a flow simulator: a) Initial b) 2 days c) 4 days d) 6 days e) 8 days f) 10 days. A: API 5L X65 B: ASTM A53-B

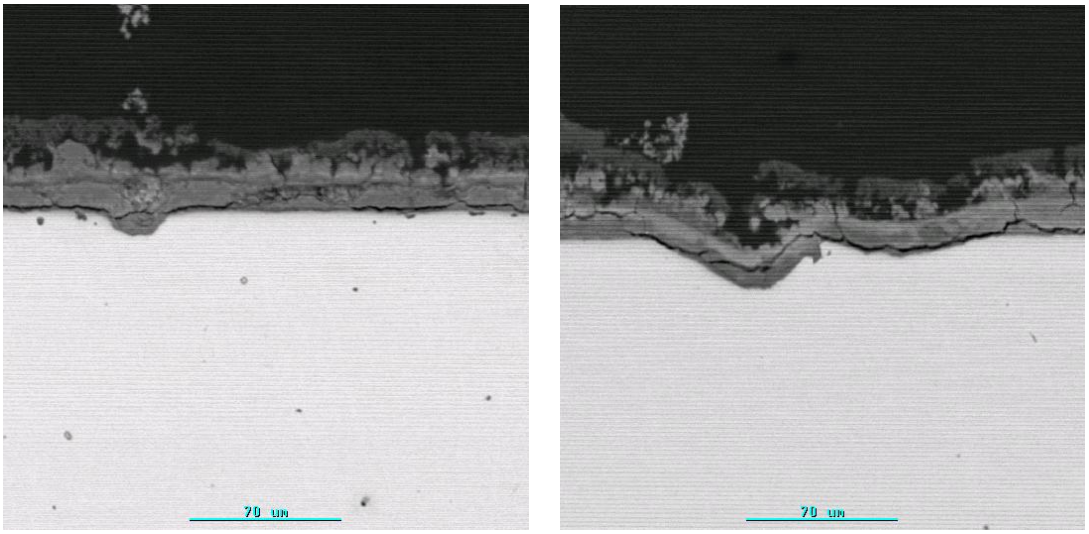

A B

Figure 8. SEM after 10 days in a flow simulator. A: API 5L X65 B: ASTM A53-B

4. CONCLUSIONS

The principal conclusions drawn from this study are the following:

- The microstructure of the API 5L X65 and ASTM A53-B steel is formed mainly of ferrite grains, with a fine grain size of ASTM 10 for the API steel and ASTM 8 for the ASTM A53-B steel.
- The average hardness measured for the API 5L X65 and ASTM A 53-B steel was 54.0 HR_A and 42.8 HR_A, respectively. This data corroborates the classification of API 5L X65 steel as a high strength pipe material, and ASTM A53 steel as a medium strength pipe material.

- The seawater used in this study has chlorinity of 19.64 g Kg^{-1}, salinity of 35.45 g Kg^{-1}, conductivity of 45.40 mS cm^{-1} and a pH of 7.73.
- The results obtained from the (static) electrochemical testing gave the variables of corrosion potential, corrosion current, corrosion rate, passivity current and pitting potential, showing better behavior for all the measurements against corrosion in seawater for the API 5L X65.
- The total corrosion rate considering the corrosion and erosion processes for the materials in a flow simulator system after 10 days of testing was 0.14 μm $year^{-1}$ for the API 5L X65 steel and 0.59 μm $year^{-1}$ for the ASTM A53-B steel. SEM observations showed preferential formation of pitting on the ASTM A53-B steel.

ACKNOWLEDGEMENTS
The authors gratefully acknowledge the support of the Dirección de Investigación at the Pontificia Universidad Católica de Valparaíso.

References

1. E. Bardal, *Corrosion and protection, Engineering Materials and Processes, 1st Edition*, Springer, London, 2004, pp. 193-218.
2. Y. Yang, Y.F. Cheng, *Wear*, 277 (2012) 141.
3. M.A. Hegazy, M. Abdallah, M.K. Awad, M. Rezk, *Corros. Sci.*, 81 (2014) 54.
4. L. Zeng, G.A. Zhang, X.P. Guo, *Corros. Sci.*, 85 (2014) 318.
5. Y. Zou, J. Wang, Q. Bai, L. L. Zhang, X. Peng, X. F. Kong, *Corros. Sci*., 57 (2012) 202.
6. R. Jeffrey, R. E. Melchers, *Corros. Sci*., 49 (2007) 2270.
7. C. Rémazeilles, Ph. Refait, *Corros. Sci*., 50 (2008) 856.
8. Y. T. Ma, Y. Li, F. H. Wang, *Corros. Sci*., 51 (2009) 997.
9. T. Nishimura, H. Katayama, K. Noda, T. Kodama, *Corrosion*, 56 (2000) 935.
10. Saleh A., Al-Fozan, Anees U. Malik, *Desalination*, 228 (2008) 61.
11. R. Mendoza, M. Alanis, R. Pérez, O. Alvarez, C. González, J. Juarez-Islas, *Mater. Sci. Eng*., 337 (2002) 115.
12. R. Mendoza, J. Huante, G. Lugo, O. Alvarez-fregozo, J. Juarez-Islas, *Mater. Sci. Perform*., 8 (1999) 549.
13. R. Mendoza, J. Huante, M. Alanis, C. González-Rivera, J. Juarez-Islas, *Mater. Sci. Eng*., 276 (2000) 203.
14. R. Mendoza, J. Huante, M. Alanis, C. González-Rivera, J. Juarez-Islas, *Mater. Process. Technol*, 101 (2000) 238.
15. B. Vargas-Arista, J. M. Hallen, A. Albiter, *Mater. Charact*., 58 (2007) 721.
16. S.D. Bhole, J.B. Nemade, L. Collins, Cheng Liu, *Mater. Process. Technol*., 173 (2006) 92.
17. G.M. Evans, N. Bailey, *Metallurgy of Basic Weld Metal*, Woodhead Publishing Limited, Cambridge, UK, 1997, pp. 161–185.
18. W. Wang, S. Liu, *Weld. J*., 81 (2002) 132.
19. S.H. Hashemi, D. Mohammadyani, *Int. J. Pres. Ves. Pip*., 98 (2012) 8.
20. A 53/A 53M-02 standard specification for pipe, Steel, black and hot-dipped, zinc-coated, welded and seamless.
21. J. Safarov, S. Berndt, F. Millero, R. Feistel, A. Heintz, E. Hassel, *Deep Sea Res. Part. 1*, 65 (2012) 146.

22. ASTM E 112-10, Standard test methods for determining average grain size.
23. ASTM D 2688-94 Standard test methods for corrosivity of wáter in the absence of heat transfer (Weight loss methods).
24. ASTM G1-03 Standard practice for preparing, cleaning and evaluating corrosion test specimens.
25. J. Soltis, *Corros. Sci.*, 90 (2015) 5.
26. El-Sayed M. Sherif, A. Abdulhakim, *Int. J. Electrochem. Sci*., 10 (2015) 34.
27. R. Vera, C. Tapia, B.M. Rosales, *Corros. Sci.*, 45 (2003) 321.
28. Z. B. Zheng, Y. G. Zheng, X. Zhou, S. Y. He, W. H. Sun, J. Q Wang, Corros. Sci., 88 (2014) 187.
29. A. Cervantes Tobón, M. Díaz Cruz, M. A. Domínguez Aguilar, J. L. González Velázquez, *Int. J. Electrochem. Sci.*, 10 (2015) 2904.